Available online at www.sciencedirect.com
ScienceDirect
Journal of Power Sources 167 (2007) 281–287
JOURNAL OF POWER SOURCES
www.elsevier.com/locate/jpowsour

Direct methanol fuel cell with extended reaction zone anode: PtRu and PtRuMo supported on graphite felt

Alex Bauer, Előd L. Gyenge *, Colin W. Oloman

Department of Chemical and Biological Engineering, The University of British Columbia, 2360 East Mall, Vancouver, BC, Canada V6T 1 Z3

Received 2 February 2007; received in revised form 22 February 2007; accepted 23 February 2007
Available online 2 March 2007

Abstract

Pressed graphite felt (thickness ~350 μm) with electrodeposited PtRu (43 g m^{-2}, 1.4:1 atomic ratio) or PtRuMo (52 g m^{-2}, 1:1:0.3 atomic ratio) nanoparticle catalysts was investigated as an anode for direct methanol fuel cells. At temperatures above 333 K the fuel cell performance of the PtRuMo catalyst was superior compared to PtRu. The power density was 2200 W m^{-2} with PtRuMo at 5500 A m^{-2} and 353 K while under the same conditions PtRu yielded 1925 W m^{-2}. However, the degradation rate of the Mo containing catalyst formulation was higher. Compared to conventional gas diffusion electrodes with comparable PtRu catalyst composition and load, the graphite felt anodes gave higher power densities mainly due to the extended reaction zone for methanol oxidation.

Keywords: Nanoparticles; Methanol oxidation; Electrodeposition; Three-dimensional electrodes

1. Introduction

Methanol has been proposed the key energy carrier and chemical raw material of the future, with production shifting increasingly toward biomass and chemical/electrochemical conversion of atmospheric CO_2 as opposed to present day technologies based on syn-gas obtained from natural gas and coal [1]. Closing the CO_2 emission loop by employing an electrochemical reactor producing CH_3OH and/or $HCOO^-$/HCOOH at the cathode [2] to be fed directly into a fuel cell anode with an overall net energy production, while still a distant goal, could represent an important advancement toward sustainable energy generation.

The issues that need to be addressed associated with direct methanol fuel cells (DMFC) are well-documented in the literature. These are (selected references are also indicated): electrocatalysis of CH_3OH oxidation (e.g. on PtRu with load typically above 10 g m^{-2}) [3–8], CH_3OH permeation through the polymer electrolyte-membrane causing a mixed cathode potential and bringing about a need for methanol tolerant O_2 electroreduction catalysts [9,10] and inefficient two-phase (liquid/gas) counter-current flow of $CH_3OH_{(aq)}$ toward and $CO_{2(g)}$ away from the catalytically active sites in the anode structure [11–13]. These problems are expected to worsen with scale-up to high power output (e.g. 100 kW range) and larger stacks, such as those required for transportation. Therefore, at present portable power applications are deemed the most feasible for commercialization of direct methanol fuel cells [14].

In order to solve these challenges it is important to recognize the interaction among the above mentioned effects such as a low methanol oxidation rate at the anode, which will lead to a high methanol concentration adjacent to the membrane causing an enhanced crossover flux to the cathode. Moreover, CO_2 gas entrapment and accumulation in the porous anode increases the pressure on the anode side and could induce both CH_3OH and CO_2 crossover.

Recently it has been proposed to replace the traditionally employed gas diffusion electrode relying on a thin (~20 μm) catalyst layer, with a three-dimensional anode (also referred to as extended reaction zone anode), having uniformly distributed catalyst nanoparticles throughout its thickness (i.e. approximately between 200 and 1000 μm depending on the type of electrode material and compression in the fuel cell) [15–17].

Most of the research to date in this area has focused on developing novel methods for nanostructured catalyst synthesis and deposition onto various three-dimensional electrodes such

* Corresponding author. Tel.: +1 604 822 3217; fax: +1 604 822 6003.
E-mail address: egyenge@chml.ubc.ca (E.L. Gyenge).

0378-7753/$ – see front matter © 2007 Elsevier B.V. All rights reserved.
doi:10.1016/j.jpowsour.2007.02.053

as pressed and uncompressed graphite felts [15,17] and reticulated vitreous carbon [16]. Therefore, the extended reaction zone concept has not been thoroughly validated yet by fuel cell experiments.

In this context, the objective of the present work was to follow up on our previous study, where we presented a novel surfactant assisted method to electrodeposit PtRu nanoparticles on pressed graphite felt (thickness ~350 μm) [15], by investigating the performance of the graphite felt anode in DMFCs in comparison with commercial gas diffusion electrodes with carbon black supported PtRu catalyst. Furthermore, the nanoparticle preparation procedure was extended to the ternary system PtRuMo and the role of Mo in the electrocatalyst formulation was studied in both half-cell and fuel cell experiments.

Interestingly, while there are a number of publications revealing the positive effect of Mo on methanol electrooxidation kinetics in half-cell experiments [18–21], there is generally a lack of longer-term fuel cell studies involving PtRuMo. Neto et al. showed by cyclic voltammetry at 293 K that PtRuMo nanoparticles prepared by a colloidal method with 1:1:1 atomic ratio gave a 100 mV lower methanol oxidation onset potential compared to PtRu (1:1) [19]. This observation is corroborated by the findings of Lima et al., who identified by in situ IR reflectance spectroscopy the presence of CO_2 from CH_3OH oxidation at a 100 mV lower potential when Mo was present in a PtRu/polyaniline catalyst. Furthermore, the same authors reported that PtRuMo was less sensitive to CO_{ad} poisoning [20]. Zhang et al. confirmed the beneficial Mo effect by chronopotentiometry at 100 A m^{-2}, reporting approximately a 50–100 mV lower anode potential in case of methanol oxidation on PtRuMo compared to PtRu [21].

Thus, in terms of the ternary catalyst composition PtRuMo, the present work attempts to bridge a gap between fundamental electrochemical investigations and fuel cell experiments.

2. Experimental

2.1. Electrodeposition

Before deposition the pressed graphite felt (5 cm^2 geometric area, 350 μm thickness, Test Solutions Inc.) was rinsed with methanol (Fisher) and deionized water followed by air drying in an oven at 333 K. The electrodeposition media contained 40 wt% Triton X-100 ($C_{14}H_{22}O(C_2H_4O)_n$, $n \approx 9.5$) (Aldrich) and metal salts: 65 mM $H_2PtCl_6 \cdot 6\,H_2O$ (99.9% Aldrich), 65 mM $RuCl_3 \cdot 3\,H_2O$ (99.9% Alfa-Aesar) while in the case of the ternary catalyst, 32.5 mM $MoCl_5 \cdot 5\,H_2O$ (98% Aldrich) was also added. The deposition was carried out twice, in galvanostatic mode at 60 A m^{-2} and 333 K for 1.5 h each utilizing a sandwich type cell with two platinized Ti plates functioning as counter electrodes. Between the first and second deposition steps the graphite felt electrode was washed with deionized water and methanol and dried in air. The temperature for both washing and drying was 333 K. The second deposition step was carried out employing fresh electrodeposition media.

After the two consecutive electrodeposition steps the felt was sonicated in methanol and rinsed thoroughly with methanol and deionized water at 333 K, followed by drying in air at 333 K. To reduce the surface oxides formed during sample treatment, electrochemical reductive cleaning of the PtRu(Mo) electrodeposited pressed felt was performed for 10 min in 0.5 M H_2SO_4 at a constant potential of −0.8 V versus Hg/Hg_2SO_4, $K_2SO_{4\,std.}$ reference electrode (abbreviated as MSE) for 10 min [E (V versus SHE) = 0.64 + E (V versus MSE)].

Scanning electron microscopy was carried out to study the deposit morphology. The catalyst loading and bulk atomic ratio were determined by digesting a sample of deposited felt in aqua regia at 363 K for 3 h followed by inductively coupled plasma atomic emission spectroscopy (ICP-AES) analysis. The effective Pt surface area was estimated by the Cu underpotential deposition and anodic stripping method [15,16,22].

2.2. Electrochemical half-cell experiments

A PARSTAT 2263 potentiostat controlled by PowerSuite® software (Princeton Applied Research) was employed. The working electrode was 1 cm^2 of pressed felt with PtRu or PtRuMo electrodeposited on it, immersed in 0.1 M H_2SO_4. Two graphite rods of 20 cm^2 total geometric area served as counter electrodes and an MSE was employed via a Luggin capillary as the reference electrode. Cyclic voltammetry was carried out in 0.1 M H_2SO_4 at 5 mV s^{-1} to provide a blank scan. Afterwards 0.5 M CH_3OH was added to the electrolyte and cyclic voltammetry and chronopotentiometry were carried out to characterize the catalyst performance. Experiments were performed at both 298 and 343 K.

2.3. Fuel cell experiments

The fuel cell performance of the catalyzed felt anodes was evaluated employing a 5 cm^2 area experimental DMFC with gold plated stainless steel end plates having serpentine type flow channels. The Nafion® 117 membrane had a 40 g m^{-2} Pt black catalyst loading on the cathode side (Lynntech Inc.). As backing/diffusion layers untreated carbon cloth and ELAT® were employed on the anode and cathode side, respectively. Temperature, oxidant flow rate, cathode backpressure and the electronic load (current) were set and controlled by the FC Power™ software associated with the Fideris Inc. test station. The cathode pressure was 2 atm (abs). Dry O_2 was supplied at a flow rate of 500 ml min^{-1} STP. The anolyte, consisting of 1 M CH_3OH in 0.5 M H_2SO_4, was circulated at 5 ml min^{-1} and ambient pressure employing a peristaltic pump.

3. Results and discussion

3.1. PtRu and PtRuMo electrodeposition on graphite felt

As shown by high resolution scanning electron microscopy, the surfactant assisted electrodeposition technique produced meso-porous PtRu and PtRuMo coatings on the fiber surface, consisting of particles and agglomerates with approximate diameters ranging from 10 to100 nm (Fig. 1). It must be noted that transmission electron microscopy images could not be obtained

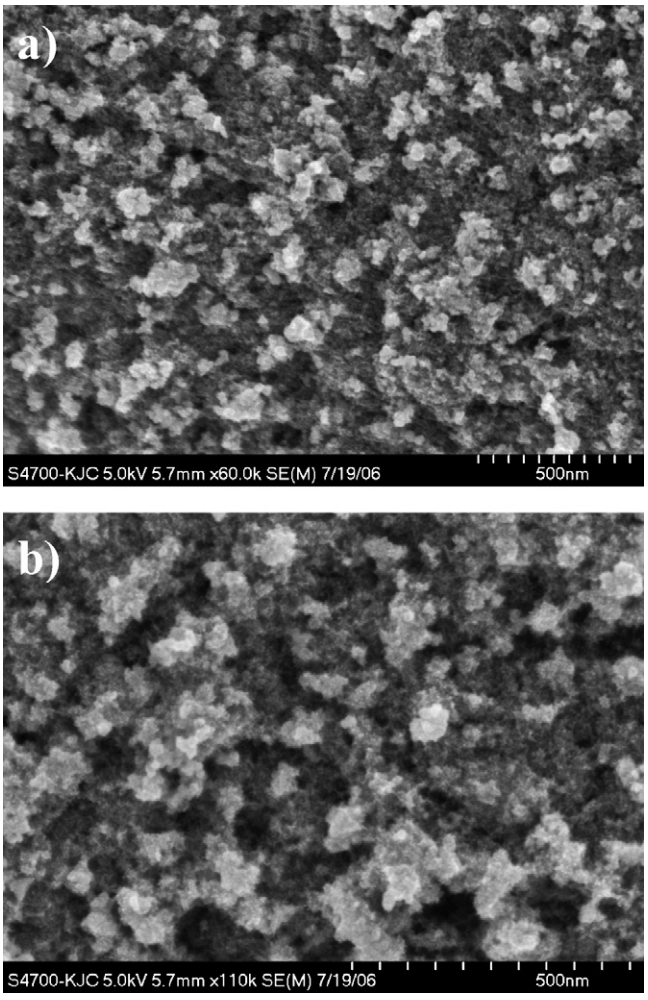

Fig. 1. HiRes SEM micrographs of PtRu (a) and PtRuMo (b) deposits on the pressed graphite fiber surface.

because slices of adequate thickness (∼100 nm) for this type of analysis could not be prepared from the catalyzed felt material.

The properties of the binary and ternary catalyst are listed in Table 1. The total catalyst load was approximately 20% higher in the case of the PtRuMo composition, while the Pt load of the two catalysts was almost identical. Interestingly, the effective Pt surface area, as determined by anodic stripping of the underpotential-deposited Cu monolayer, was almost three times lower in case of PtRuMo compared to PtRu (Table 1). This indicates extensive surface segregation of Mo in the ternary catalyst formulation.

Table 1
Physico-chemical characteristics of the binary and ternary catalysts electrodeposited on the pressed felt by the Triton X-100 assisted method

Physico-chemical property	Pt:Ru	Pt:Ru:Mo
Atomic ratio	1.4 : 1	1:1:0.3
Total catalyst load [g m_{felt}^{-2}]	43	52
Pt load [g m_{felt}^{-2}]	32	32
Effective Pt surface area [m^2 m_{felt}^{-2}]	712	254
Mass specific Pt surface area [m^2 g_{Pt}^{-1}]	23	8

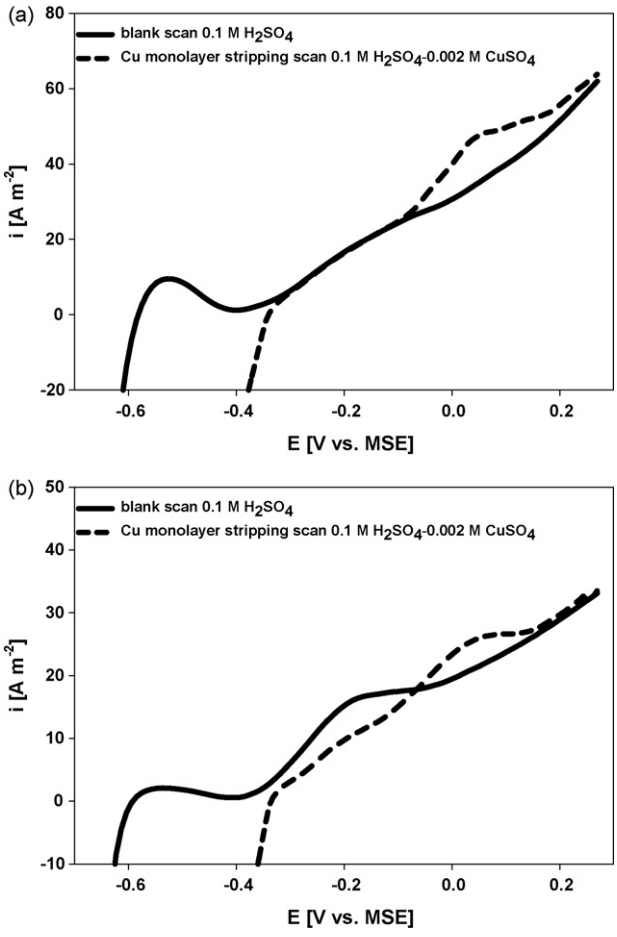

Fig. 2. Anodic stripping of the underpotential-deposited Cu monolayer on the graphite felt electrode with PtRu (a) and PtRuMo (b). Scan rate 0.5 mV s^{-1}.

Fig. 2 shows the Cu stripping voltammograms used for the effective surface area calculation. Moreover, the blank scan in 0.1 M H_2SO_4 conducted with the Mo containing catalyst showed an anodic peak at −0.2 V versus MSE, indicating Mo oxidation (compare Fig. 2b and a). It is noteworthy that Cu did not underpotential-deposit on Mo, therefore, its surface area could not be determined by the employed method. In separate experiments utilizing only Ru catalyst supported on graphite felt, a pronounced stripping peak at −0.26 V versus MSE was obtained. However, when the method was applied to either PtRu or PtRuMo, it did not yield a distinct peak in the potential range related to Ru (i.e. between −0.34 V versus MSE and −0.17 V versus MSE). This result is consistent with the findings of Cheng and Gyenge regarding PtRu supported on reticulated vitreous carbon [16]. It is therefore assumed that the area determined by Cu UPD and stripping reflects the active Pt area of the respective binary and ternary catalyst formulations.

3.2. Effect of Triton X-100 on the electrodeposition of Pt, Ru and Mo on graphite felt

In order to obtain information regarding the influence of Triton X-100 on the electrodeposition of the various metal ions, cathodic polarization experiments were carried out at 333 K

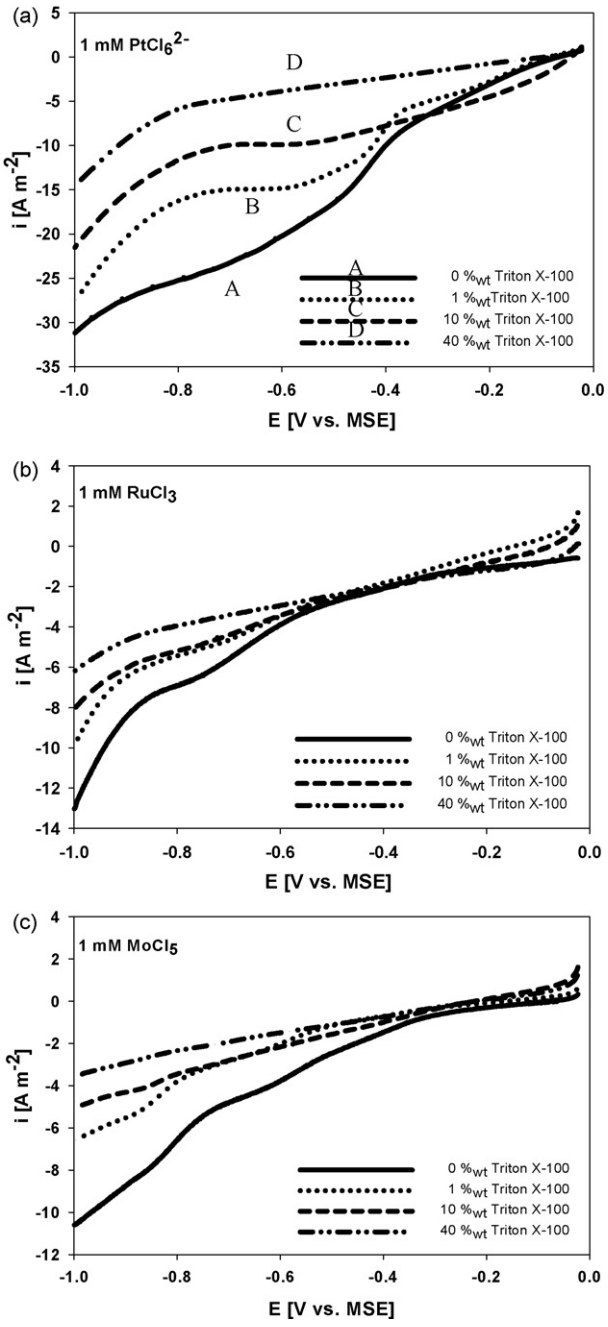

Fig. 3. Effect of Triton X-100 on the voltammogram of Pt (a), Ru (b) and Mo (c) electrodeposition on graphite felt. Scan rate 5 mV s^{-1}.

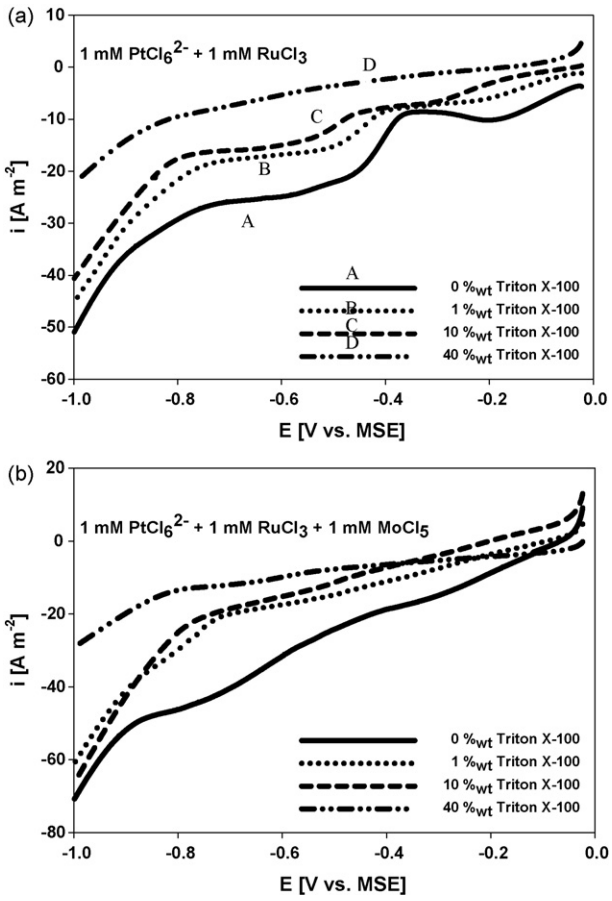

Fig. 4. Effect of Triton X-100 on the voltammogram of PtRu (a) and PtRuMo (b) codeposition on graphite felt. Scan rate 5 mV s^{-1}.

and 5 mV s^{-1} on 1 cm^2 pressed felt in the metal salt solutions, H_2PtCl_6, $RuCl_3$ and $MoCl_5$ both individually (Fig. 3) and in combination (Fig. 4). The concentration of each metal species was 1 mM.

Fig. 3 shows the scans for the individual metal depositions. In the absence of surfactant, for all three species essentially two cathodic waves can be distinguished. At potentials more positive than −0.8 V versus MSE, primarily the electrodeposition of Pt, Ru and Mo takes place, while at more negative potentials the secondary reaction of H_2 evolution gains significance, thereby, lowering the deposition current efficiency. In the potential domain of interest, i.e. between −0.4 and −0.8 V versus MSE where the metal deposition occurs with high current efficiency, the largest cathodic current was obtained for $PtCl_6^{2-}$. Thus, as discussed also previously [15], in the absence of Triton X-100 the electrodeposition of Pt is favored forming a Pt-rich catalyst on the graphite felt.

The gradual increase of Triton X-100 concentration from 0 to 40 wt% resulted in a significant decrease of the Pt deposition current density (Fig. 3a). At 40 wt% Triton X-100 the Pt deposition polarization curve became linear up to −0.8 V with a large dE/di ratio (Fig. 3a). This is due to the large crystallization overpotential as a result of low ad-atom surface diffusivity on the surfactant-covered surface [23], leading to isolated nuclei formation followed by restricted growth of nuclei to three-dimensional crystallites and possible coalescence into larger aggregates (nucleation-coalescence mechanism for electrodeposition).

The effect of surfactant on the electrodeposition current of either Ru or Mo was less pronounced compared to Pt (compare Fig. 3a–c). This indicates that the electroreduction kinetics of both Ru and Mo ions are slow, hence, their deposition current density was less affected by ad-atom diffusion limitation and restricted growth effects.

Fig. 4 shows the voltammograms obtained for codeposition of PtRu (Fig. 4a) and PtRuMo (Fig. 4b), respectively. In the case of both PtRu and PtRuMo, without surfactant present in the depo-

sition bath the codeposition current at potentials between −0.6 and −0.8 V (Fig. 4) is fairly close to the sum of the individual deposition currents of the constituent elements, therefore, a Pt-rich catalyst would be generated (Fig. 3a–c). With 40 wt% Triton X-100, while the codeposition current is again approximately equal to the sum of the individual deposition currents of the respective elements, due to the low Pt deposition current (Fig. 3a), the ratio of the co-deposited elements is different. Therefore, the presence of surfactant was crucial to control the Pt:Ru and Pt:Ru:Mo atomic ratio in the deposit, by selectively lowering the Pt deposition current density compared to Ru and Mo (Fig. 3a–c).

In the case of the PtRu codeposition without Triton X-100 (Fig. 4a) a nucleation peak was observed at −0.2 V as well as a shoulder wave between −0.45 and −0.55 V, which represents crystal growth. When the surfactant concentration was increased to 1 and 10 wt% nucleation became more difficult as indicated by the shift of the nucleation wave to more negative potentials. At 40 wt% Triton X-100 both the nucleation and growth peaks disappeared due to isolated nucleation sites, low surface diffusivity of ad-atoms and restricted growth.

3.3. Methanol electro-oxidation experiments

Cyclic voltammograms for methanol oxidation on PtRu and PtRuMo are presented in Fig. 5, at 298 and 343 K, respectively. The forward (anodic) scans were virtually identical with the reverse (cathodic) scans, therefore, only the former are presented.

At 298 K the PtRu catalyst yielded significantly higher oxidation currents than PtRuMo. This can be explained in part by the larger Pt surface area of the PtRu catalyst (Table 1) available for methanol adsorption. It has been established that at low temperatures (e.g. 298 K) methanol adsorption and dehydrogenation is not favored on Ru. This was elegantly shown by first principle quantum mechanics calculation of binding energies and heats of formation [24]. It is unknown, however, whether methanol

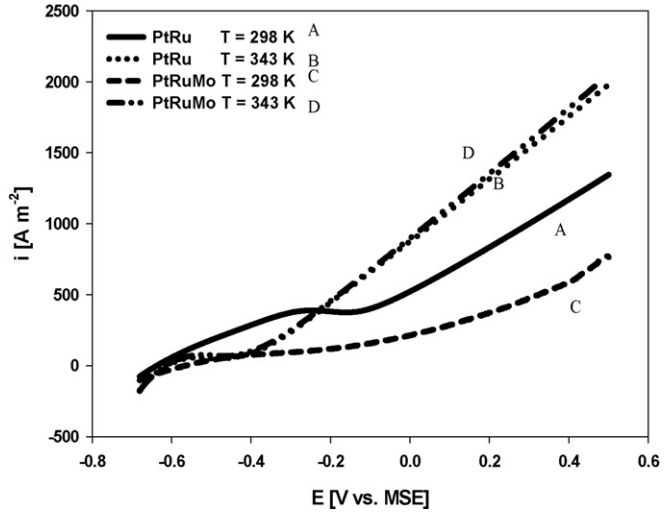

Fig. 5. Voltammogram of methanol electro-oxidation using PtRu and PtRuMo catalysts deposited on compressed felt: 0.5 M CH_3OH–0.1 M H_2SO_4, 5 mV s^{-1}.

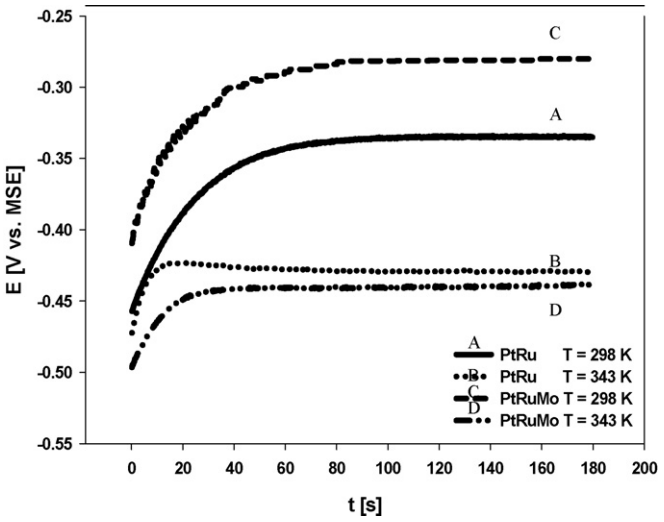

Fig. 6. Chronopotentiometry of methanol electro-oxidation using PtRu and PtRuMo catalysts deposited on compressed felt: 0.5 M CH_3OH–0.1 M H_2SO_4, 50 A m^{-2}.

adsorbs on Mo, which is thought to have bifunctional properties similar to Ru, hence, facilitating the formation of OH_{ad} [25]. Furthermore, the role of Mo has been also explained based on the assumption that the activation barrier for the oxidation of CO_{ad} is lowered due to an oxygen spillover effect [26].

Increasing the temperature from 298 to 343 K had the most pronounced effect on the Mo containing catalyst, enhancing the CH_3OH oxidation superficial current density by up to five or six times at potentials more positive than −0.4 V versus MSE (Fig. 5).

Additionally, chronopotentiometry of methanol oxidation was performed on the two catalysts at 298 and 343 K, respectively (Fig. 6). The latter experiment is more relevant for fuel cell operation compared to cyclic voltammtery, since it simulates the anode potential variation in time at a constant current density. In accordance with the cylic voltammetry data, at 298 K and 50 A m^{-2} the anode potential of the PtRuMo catalyst was more positive by about 60 mV. However, at 343 K an approximately 10–30 mV lower anode potential was obtained with the Mo containing catalyst (Fig. 6), while having the same Pt load for both catalyst formulations (Table 1). Thus, there is a strong interaction effect between the presence of Mo and temperature. Addition of Mo to the PtRu catalyst formulation is beneficial only at higher temperatures such as 343 K and above. The positive interaction effect between temperature and Mo content seems to follow the observation of Dickinson et al. regarding Ru, in that a higher Ru content (i.e. PtRu ratio of 1:1 versus 1.5:1) enhanced the anode performance at high temperatures (e.g. 338 K) [27]. This is related to the rate determining step shift from CH_3OH adsorption/dehydrogenation at low temperatures to the reaction of CO_{ad} with OH_{ad} at high temperatures.

3.4. Fuel cell experiments

Fuel cell polarization curves were obtained for the two pressed graphite felt supported catalysts (PtRu and PtRuMo,

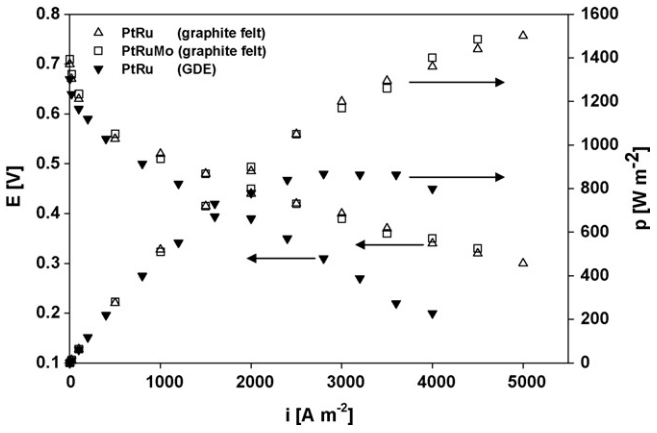

Fig. 7. Fuel cell polarization experiments at 333 K. Anode comparison: commercial gas diffusion electrode vs. PtRu and PtRuMo deposited onto pressed felt. Anode feed: 1 M CH_3OH–0.5 M H_2SO_4, 5 ml min^{-1}, ambient pressure; cathode feed: dry O_2, 500 ml min^{-1} STP, 2 atm.

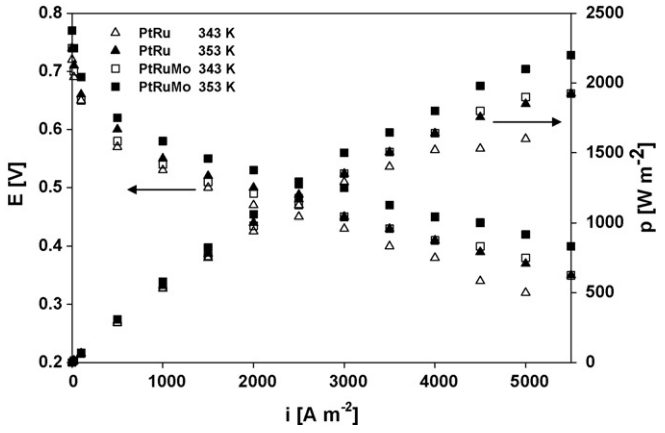

Fig. 8. Fuel cell polarization experiments at 343 and 353 K using the pressed felt supported PtRu and PtRuMo catalysts. Anode feed: 1 M CH_3OH–0.5 M H_2SO_4, 5 ml min^{-1}, ambient pressure; cathode feed: dry O_2, 500 ml min^{-1} STP, 2 atm.

respectively) as well as for a commercially available PtRu gas diffusion electrode (GDE) of comparable load and composition (40 g m^{-2}, 1:1 atomic ratio) (Lynntech Inc.).

Fig. 7 compares the performance of the gas diffusion electrode with pressed felt at 333 K. At the latter temperature there was virtually no difference between the PtRu and PtRuMo catalysts electrodeposited on graphite felt, supporting therefore, the conclusions of the voltammetry and chronopotentiometry experiments. However, the pressed felt electrodes gave significantly better performance compared to the gas diffusion electrode. The open circuit voltage was 0.67 V for the commercial electrode and 0.70–0.71 V for the graphite felt supported PtRu and PtRuMo containing anodes. Furthermore, at 3000 A m^{-2} and 333 K the fuel cell power density was enhanced by 38% with the pressed felt anode, from 870 W m^{-2} (i.e. peak power for the GDE) to 1200 W m^{-2}. The maximum power output of the novel extended reaction zone anode was about 1500–1600 W m^{-2}.

It must be noted that the performance of the reference GDE can be considered representative of the state-of-the-art of these electrode types. In the literature, for GDEs with carbon black (Vulcan XC-72) supported PtRu anode catalysts of 40–50 g m^{-2} load, peak power outputs at 333 K of 250 W m^{-2} [28], 600–750 W m^{-2} [29] and 1000 W m^{-2} [30] were reported. Therefore, it can be stated that the extended reaction zone anode gave clearly a better performance. This can be most likely attributed to the higher utilization of the nanoparticle catalyst, as shown also by Lycke and Gyenge for direct ethanol fuel cells [17]. Moreover, although not proven experimentally yet, it is proposed that the extended reaction zone lowers the methanol crossover rate. Thereby, the negative effect of the mixed cathode potential is to some extent mitigated.

Due to the novelty of the employed anode design, there are very few literature results that could be used for comparison. Scott and co-workers reported DMFC polarization curves using PtRu (10 g m^{-2}, 1:1 atomic ratio) supported on Ti mesh, which could be also considered a three-dimensional extended reaction zone electrode type. The Ti mesh anode gave virtually no improvement compared to a conventional gas diffusion electrode, having a power output of 600 W m^{-2} at 3000 A m^{-2} and 363 K [31].

Fig. 8 shows that the Mo presence in the catalyst formulation of the pressed felt anode was beneficial for the fuel cell power output at higher temperatures (i.e. especially at 353 K) in agreement with the voltammetric and chronopotentiometric experiments.

At 343 and 353 K the open circuit voltages were 0.72 and 0.74 V without Mo and 0.74 and 0.77 V when using PtRuMo, respectively. At a current density of 5500 A m^{-2} and 353 K the power density with the PtRuMo catalyst was 2200 W m^{-2} while the binary PtRu catalyst yielded 1925 W m^{-2} (Fig. 8).

We could find only one literature report on the activity of PtRuMo utilized in a DMFC. Employing 20 g m^{-2} PtRuMo dispersed on polyaniline, Lima et al. obtained a peak power output of only about 200 W m^{-2} at 383 K [18], i.e. about an order of magnitude lower than in the present work carried out at 353 K. Thus, it can be stated that the interaction between the pressed graphite felt support and either PtRu or PtRuMo points toward a promising direction in the effort of improving the power output of DMFCs. Moreover, the three-dimensional electrode design presented here could be advantageous for flow-through mixed reactant DMFCs [32].

3.5. Fuel cell anode durability

Generally, very few literature reports show the performance of direct fuel cells over extended periods of time. Performance evaluations are typically made based on polarization curves, which are recorded over a time frame of less than an hour. To address this issue in the present work, a constant superficial current density of 4000 A m^{-2} was applied for 3 h to monitor the anode catalyst deactivation during fuel cell operation at 353 K (Fig. 9). While the PtRuMo catalyst performed better during polarization experiments, its cell voltage decreased at a higher rate. Assuming an approximately linear correlation between voltage loss and time, the degradation rate was 26 mV h^{-1} in the case of PtRuMo and 13 mV h^{-1} for PtRu, respectively.

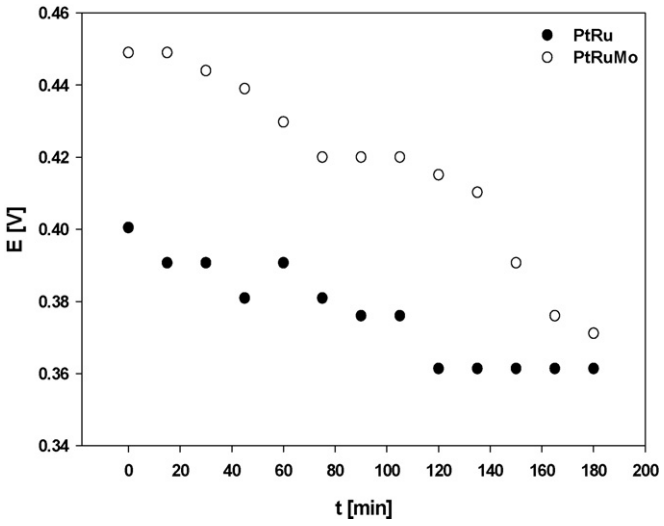

Fig. 9. Longer-term fuel cell polarization experiments at 4000 A m^{-2} and 353 K. Pressed felt anode with PtRuMo and PtRu. Conditions identical to Fig. 8.

After 3 h of continuous operation the cell voltages for PtRuMo and PtRu became almost identical due to degradation of the PtRuMo anode performance, whilst the cell voltage with the PtRu catalyst stabilized after 2 h (Fig. 9). The lower stability of PtRuMo could be explained by possible Mo oxidation to Mo^{3+} as suggested also by the voltammogram in 0.1 M H_2SO_4 (Fig. 2b).

4. Conclusions

Surfactant assisted galvanostatic electrodeposition of PtRu and PtRuMo onto pressed graphite felt (thickness 350 μm) yielded particles and agglomerates of ∼10–100 nm diameter. Fuel cell polarization experiments revealed a significant improvement in power output with the extended reaction zone graphite felt anode compared to a conventional gas diffusion electrode having approximately the same Pt loading. At 3000 A m^{-2} and 333 K the fuel cell power density was enhanced by 38% with the novel anode. The PtRuMo catalyst showed a strong positive interaction effect with temperature, performing better than PtRu at higher temperatures, such as 343 and 353 K, respectively. The power density obtained with PtRuMo supported on pressed graphite felt was 2200 W m^{-2} at 3000 A m^{-2} and 353 K. However, a higher anode catalyst degradation rate was observed for the Mo containing catalyst. Therefore, this work showed that Mo based anode catalysts could be practical in DMFCs only if an adequate catalyst regeneration method could be devised or a more stable alloy formulation could be identified.

Acknowledgments

The authors gratefully acknowledge the financial support of the BC Advanced Systems Institute and the Natural Sciences and Engineering Research Council of Canada.

References

[1] G. Olah, A. Goeppert, G.K. Surya Prakash, Beyond Oil and Gas: The Methanol Economy, Wiley-VCH Verlag GmbH & Co., Weinheim, 2006.
[2] H. Li, C. Oloman, J. Appl. Electrochem. 36 (2006) 1105.
[3] H.A. Gasteiger, N. Markovic, P.N. Ross, E.J. Cairns, J. Phys. Chem. 97 (1993) 12020.
[4] T. Iwasita, H. Hoster, A. John-Anacker, W.F. Lin, W. Vielstich, Langmuir 16 (2000) 522.
[5] D. Cao, G.-Q. Lu, A. Wieckowski, S.A. Wasilevski, M. Neurock, J. Phys. Chem. B 109 (2005) 11622.
[6] C. Bock, B. MacDougall, Y. LePage, J. Electrochem. Soc. 151 (2004) A1269.
[7] H. Wang, C. Wingender, H. Baltruschat, M. Lopez, M.T. Reetz, J. Electroanal. Chem. 509 (2001) 163.
[8] J. Jiang, A. Kucernak, J. Electroanal. Chem. 543 (2003) 187.
[9] B. Gurau, E.S. Smotkin, J. Power Sources 112 (2002) 339.
[10] J.L. Fernandez, V. Raghuveer, A. Manthiram, A.J. Bard, J. Am. Chem. Soc. 127 (2005) 13100.
[11] P. Argyropoulos, K. Scott, W.M. Taama, J. Appl. Electrochem. 29 (1999) 661.
[12] W.M. Yang, S.K. Chou, C. Shu, J. Power Sources 164 (2007) 549.
[13] T. Schultz, U. Krewer, T. Vidakovic, M. Pfafferodt, M. Christov, K. Sundmacher, J. Appl. Electrochem. 37 (2007) 111.
[14] C.Y. Chen, J.Y. Shiu, Y.S. Lee, J. Power Sources 159 (2006) 1042.
[15] A. Bauer, E.L. Gyenge, C.W. Oloman, Electrochim. Acta 51 (2006) 5356.
[16] T.T. Cheng, E.L. Gyenge, Electrochim. Acta 51 (2006) 3904.
[17] D.R. Lycke, E.L. Gyenge, Electrochim. Acta 52 (2007) 4287.
[18] A. Lima, C. Coutanceau, J.-M. Leger, C. Lamy, J. Appl. Electrochem. 31 (2001) 379.
[19] A.O. Neto, E.G. Franco, E. Arico, M. Linardi, E.R. Gonzales, J. Eur. Ceram. Soc. 23 (2003) 2987.
[20] A. Lima, F. Hahn, J.-M. Leger, Russ. J. Electrochem. 40 (2004) 326.
[21] X. Zhang, F. Zhang, K.-Y. Chan, J. Mater. Sci. 39 (2004) 5845.
[22] C.L. Green, A. Kucernak, J. Phys. Chem. B 106 (2002) 1036.
[23] H. Fischer, Angew. Chem. Int. Ed. Engl. 8 (1969) 108.
[24] J. Kua, W.A. Goddard III, J. Am. Chem. Soc. 121 (1999) 10928.
[25] H. Bolivar, S. Izquierdo, R. Tremont, C.R. Cabrera, J. Appl. Electrochem. 33 (2003) 1191.
[26] G. Samjeske, H. Wang, T. Löffler, H. Baltruschat, Electrochim. Acta 47 (2002) 3681.
[27] A.J. Dickinson, L.P.L. Carrette, J.A. Collins, K.A. Friedrich, U. Stimming, J. Appl. Electrochem. 34 (2004) 975.
[28] C. Coutanceau, A.F. Rakotondrainibe, A. Lima, E. Garnier, S. Pronier, J.-M. Leger, C. Lamy, J. Appl. Electrochem. 34 (2004) 61.
[29] V. Baglio, A. Di Blasi, E. Modica, P. Creti, V. Antonucci, A.S. Arico, Int. J. Electrochem. Sci. 1 (2006) 71.
[30] http://www.etek-inc.com/pdfs/MEASeries12D-W.pdf.
[31] R.G. Allen, C. Lim, L.X. Yang, K. Scott, S. Roy, J. Power Sources 143 (2005) 142.
[32] M.A. Priestnall, V.P. Kotzeva, D.J. Fish, E.M. Nilsson, J. Power Sources 106 (2002) 21.